UDC 621.791.725, 669.017.165
https://doi.org/10.17073/0021-3438-2023-2-57-73

Research article
Научная статья

Structure and mechanical properties of welded joints from alloy based on VTI-4 orthorhombic titanium aluminide produced by pulse laser welding

S.V. Naumov[1], D.O. Panov[1], R.S. Chernichenko[1], V.S. Sokolovsky[1], E.I. Volokitina[1], N.D. Stepanov[1], S.V. Zherebtsov[1], E.B. Alekseev[2], N.A. Nochovnaya[2], G.A. Salishchev[1]

[1] **Belgorod State University**
85 Pobeda Str., Belgorod, 308015, Russia

[2] **Federal State Unitary Enterprise "All-Russian Scientific Research Institute of Aviation Materials" (VIAM)**
17 Radio Str., Moscow 105005, Russia

✉ Stanislav V. Naumov (NaumovStanislav@yandex.ru)

Abstract: Ti_2AlNb-based alloys are promising materials for operation at high temperatures in aerospace industry. Meanwhile, the existing difficulties of weldability restrict opportunities of their application. This work is devoted to studies of welded joints from Ti_2AlNb-based VTI-4 alloy, obtained using pulsed laser welding (PLW). The optimum PLW modes have been determined providing uniform faultless joint. The features of formation of external defects, internal pores, cracks and non-uniform penetration depth were detected depending on welding conditions. The main PLW parameters influencing on formation of welded joint are voltage and duration of laser pulse. It was demonstrated that at insufficient medium and high peak powers sawtooth seam roots and internal pores can be formed. However, at higher rates of energy input thermal hydraulic processes in welding bathe are violated, accompanied by metal splashing (spattering), heterogeneity of pulse imposition is observed. This leads to formation of cracks, higher porosity, heterogeneity of melting zone, and as a consequence, poor mechanical properties. Microstructure analysis of the welded joints obtained by means of PLW has demonstrated that the melting area is comprised of long dendritic grains of β phase, and the heat affected zone from two regions of β + α_2 phases and β + α_2 + O phases. Herewith, the achieved joint strength equals to ~80 % of the base metal produced using the optimum PLW mode.

Keywords: Ti_2AlNb-based alloy, forging, pulsed laser welding, welded joint, EBSD analysis, mechanical properties

Acknowledgments: This work was supported by the Russian Science Foundation (Agreement No. 19-79-30066) using the equipment of BSU Shared Research Facilities "Technologies and Materials".

For citation: Naumov S.V., Panov D.O., Chernichenko R.S., Sokolovsky V.S., Volokitina E.I., Stepanov N.D., Zherebtsov S.V., Alekseev E.B., Nochovnaya N.A., Salishchev G.A. Structure and mechanical properties of welded joints from alloy based on VTI-4 orthorhombic titanium aluminide produced by pulse laser welding. *Izvestiya. Non-Ferrous Metallurgy*. 2023;29(2):57–73.
https://doi.org/10.17073/0021-3438-2023-2-57-73

Структура и механические свойства сварных соединений из сплава на основе орторомбического алюминида титана ВТИ-4, полученных импульсной лазерной сваркой

С.В. Наумов[1], Д.О. Панов[1], Р.С. Черниченко[1], В.С. Соколовский[1], Е.И. Волокитина[1], Н.Д. Степанов[1], С.В. Жеребцов[1], Е.Б. Алексеев[2], Н.А. Ночовная[2], Г.А. Салищев[1]

[1] **Белгородский государственный национальный исследовательский университет**
308015, Россия, г. Белгород, ул. Победы, 85

[2] **Всероссийский научно-исследовательский институт авиационных материалов (ВИАМ)**
105005, Россия, г. Москва, ул. Радио, 17

✉ Станислав Валентинович Наумов (NaumovStanislav@yandex.ru)

Аннотация: Деформируемые сплавы на основе Ti_2AlNb с повышенной технологичностью для изготовления листовых изделий являются перспективными материалами для работы при высоких температурах в аэрокосмической отрасли, однако возникающие трудности со свариваемостью ограничивают возможности их применения. Работа посвящена изучению сварных соединений из сплава ВТИ-4 на основе Ti_2AlNb, полученных с использованием импульсной лазерной сварки (ИЛС). Определены оптимальные режимы ИЛС, обеспечивающие равномерный бездефектный шов. Выявлены особенности образования внешних дефектов, внутренних пор, трещин и неравномерности глубины проплавления в зависимости от условий сварки. Основными параметрами ИЛС, влияющими на формирование сварного шва, являются напряжение и длительность импульса лазерного излучения. Показано, что при недостаточных средней и высокой пиковых мощностях возможно образование пилообразного корня сварного шва и внутренних пор. Однако при увеличенных погонных энергиях нарушаются термогидравлические процессы в сварочной ванне, что влечет за собой выплеск металла (разбрызгивание), наблюдается неравномерность наложения импульсов. Это приводит к образованию трещин, повышенной пористости, неоднородности зоны плавления и, как следствие, к низким механическим свойствам. Микроструктурное исследование сварных соединений из сплава ВТИ-4, полученных с использованием ИЛС, показало, что зона плавления состоит из крупных дендритных зерен β-фазы, а зона термического влияния – из двух областей β + α_2-фаз и β + α_2 + O-фаз. При этом достигнута прочность ~80 % от прочности основного металла сварного соединения из сплава ВТИ-4, полученного по оптимальному режиму ИЛС.

Ключевые слова: сплав на основе орторомбического алюминида титана, ВТИ-4, Ti_2AlNb, ковка, импульсная лазерная сварка (ИЛС), сварной шов (СШ), BSE анализ, EBSD анализ, механические свойства

Благодарности: Работа выполнена при финансовой поддержке РНФ (Соглашение № 19-79-30066) с использованием оборудования Центра коллективного пользования «Технологии и материалы НИУ “БелГУ”»).

Для цитирования: Наумов С.В., Панов Д.О., Черниченко Р.С., Соколовский В.С., Волокитина Е.И., Степанов Н.Д., Жеребцов С.В., Алексеев Е.Б., Ночовная Н.А., Салищев Г.А. Структура и механические свойства сварных соединений из сплава на основе орторомбического алюминида титана ВТИ-4, полученных импульсной лазерной сваркой. *Известия вузов. Цветная металлургия*. 2023;29(2):57–73. https://doi.org/10.17073/0021-3438-2023-2-57-73

Introduction

Ti_2AlNb-based alloys, for instance, Grade VTI-4, are characterized by low weight and are promising materials for operation at higher temperatures in aircraft and aerospace industry due to their low density, high specific strength and superior resistance against oxidation and creeping [1, 2]. In addition, they can run at higher temperatures in comparison with titanium alloys and their density is by ~40 % lower than that of superalloys based on Ni (5.1 g/cm^3 against 7.7—9.0 g/cm^3) [3—5]. At the same time, the technological properties of these

alloys (for instance, weldability) restrict opportunities of their application.

The strength of a welded joint of the Ti_2AlNb-based alloys exposed to argon arc welding barely achieves 80 % of that of the base metal [6]. Herewith, the plasticity of a welded joint (WJ) decreases, coarse dendritic structure is formed, and the action of electric arc of argon welding forms wide melting area (MA) and heat affected zone (HAZ) [7, 8], which leads to a deterioration of mechanical properties. The highly concentrated heating sources applied upon laser beam welding (LBW) or electron beam welding (EBW) with optimum technological parameters and subsequent thermal treatment can provide production of faultless high-strength WJ [9—12]. This is related with the fact that the heat input and its resulting influence on a microstructure of the base metal can be reduced to minimum during these processes [13].

LBW of titanium alloys, including Ti_2AlNb-based alloys [3, 14, 15], with repetitively pulsed laser Nd:YAG (PLW) produces WJ with good surface quality, minimum defects and superior comprehensive mechanical properties. WJ quality depends on such PLW parameters as traveling speed and average power of laser, energy and duration of pulse, average peak power density, laser spot surface area, and others. The numerous performances of PLW make it possible to control heat release with the accuracy unavailable previously for continuous LBW, and also allow a wide range of experimental conditions to be applied. This can influence on the size of MA dendritic structure, as well as the grain size of various areas of welded joint in general [16, 17]. On the other hand, controlling such high number of parameters complicates the PLW processing [17]. Finally, the violation of the processing can lead to cracking or pores formation [18, 19].

Despite the advantages of LBW and EBW, welding involving highly concentrated heating sources are accompanied by metal melting and formation of columnar B2 structure [13]. In addition, one of the main problems of PLW of titanium alloys is porosity [20]. It has been reported [21] that its formation during PLW is related with the dynamics of welding bath. This is influenced by welding process variables, destruction of keyhole, and solidification processes [22]. In addition, at a high temperature gradient in a liquid bath the protection has cannot escape after rapid solidification and forms a cavity in the seam root. The influence of a plasma channel is also known. Upon violation of welding this can lead to formation of vacuum pore in WJ [23]. In addition, formation of porosity in WJ is influenced by hydrogen [23—26] and evaporation of aluminum during welding [27]. Therefore, the production of faultless WJ from Ti_2AlNb-based alloys on is a complicated problem which requires for selection process variables of PLW. Thus, this work is devoted to determination of the influence of PLW process variables on geometrical sizes and defect structure of welded joints, structure and mechanical properties of WJ from a Ti_2AlNb-based alloy.

Experimental

The material for forging operations and subsequent welding procedures was presented from a plate of the Ti_2AlNb-based VTI-4 alloy (its chemical composition, at.%: Ti—23Al—23Nb—1.4V—0.8Zr—0.4Mo—0.4Si) obtained by triple remelting in a vacuum arc skull furnace. The multiaxial deformation of workpieces cut out from this plate with the sizes of 40×30×60 mm was achieved using a DEVR 1000 modified press (Russia) equipped with a MikroInstrument Miterm T3 heating furnace (Russia). During forging, the temperature of dies was 965 ± 5 °C. The preheating of workpiece to 970 °C was carried out in a Nabertherm furnace, mod. No. 321 400v3/N/PE (Germany) in 30 min. The multiaxial forging was comprised of *abc* deformation (Fig. 1, *a*) at the speed of <0.1 mm/s, i.e. consecutively in the directions of axes *a*, *b* and *c* with the deformation degree of 50 % in each case. In order to obtain hexagonal profile, at the last stage the obtained rectangle was drawn at the edges by 7 ± 2 mm. The forged workpiece was subsequently cooled in air. The external view of the workpiece after deformation is illustrated in Fig. 1, *b*.

The PLW was carried out using a LAT-S-300 laser facility (Russia) with repetitively pulsed impact of Nd:YAG laser (1.064 μm) equipped with an L-5010-A automated coordinate table and a L-101-ChPU controller. Samples in the form of plates with the sizes of 24 × 12.5 × 1.5 mm from the VTI-4 alloy were exposed to single side butt welding. The welding joints were selected in the voltage ranges of 280—320 V and pulse duration of 3—6 ms:

- rectangular pulse with the step between pulses of 0.25 mm;
- flow rate of protecting gas Q_g = 2.5 bar (argon 4.8);
- axial gas supply along the direction of laser radiation with holding of 5 s before start of welding;
- water flow rate Q_w = 0.5 m^3/h;
- focal distance: 0.0 mm (on the surface of welded workpieces);
- welding speed: 0.3 m/min.

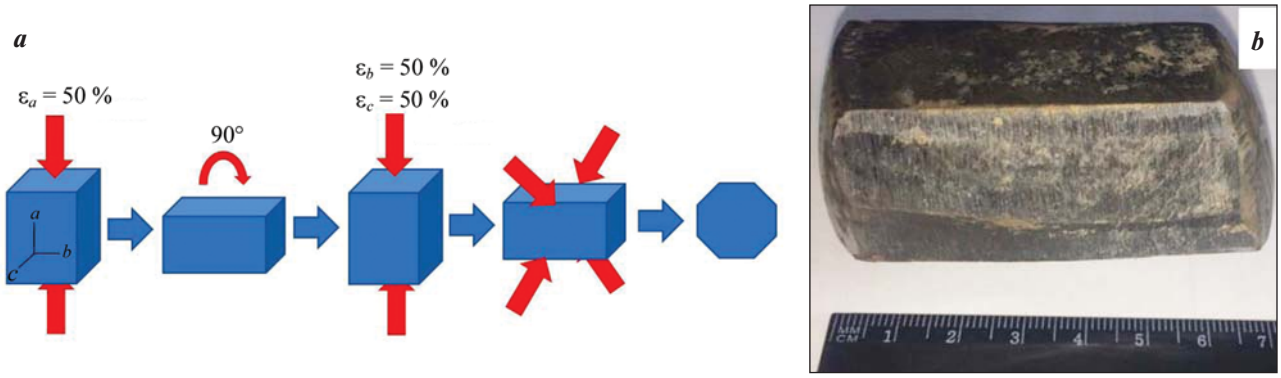

Fig. 1. Multiaxial forging of the VTI-4 alloy on a DEVR 1000 modified press
a – forging sequence; ***b*** – appearance of the forging obtained in the range t = 950÷975 °C

Рис. 1. Мультиосевая ковка сплава ВТИ-4 на модифицированном прессе DEVR 1000
a – схема ковки; ***b*** – внешний вид поковки, полученной в интервале t = 950÷975 °C

Depending on the welding mode (see Table) the peak power (P_{peak}) was varied from 2.17 to 3,21 kW, the average power was P_{avg} = 32÷90 W (Fig. 2). The PLW modes underwent preliminary testing on plates of the VTI-4 alloy. Herewith, the welding parameters were varied in a wider range. In addition, welding voltage and speed were selected on the basis of previous results [3, 14].

Samples for welding and subsequent mechanical tests were cut out using a Sodick VL400Q electric erosion machine (China) in accordance with the layout illustrated in Fig. 3, *a*. The surfaces of cutout plates before welding (24 × 12.5 × 1.5 mm) were polished using Struers SiC FEPA emery paper with a grain size of P220 (68 μm), and the surfaces of welded edges were polished using emery paper with the grain size P1000 (18 μm).

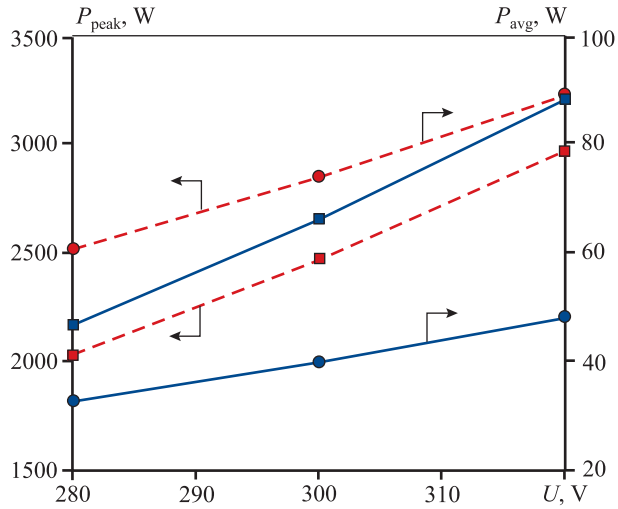

Fig. 2. Energy parameters of pulsed laser beam welding modes
τ = 3 ms (solid lines), τ = 6 ms (dashed lines)

Рис. 2. Энергетические параметры режимов ИЛС
τ = 3 мс (сплошные линии), τ = 6 мс (штриховые)

Modes of pulsed laser welding of VTI-4 alloy

Режимы импульсной лазерной сварки сплава ВТИ-4

PLW mode No.	Voltage U, V	Pulse duration τ, ms
1	280	3
2	300	3
3	320	3
4	280	6
5	300	6
6	320	6

The surfaces of samples for mechanical tests and microstructural studies were prepared also using emery paper with a grain size of P220 to P2000 (5—7 μm) at Baipol Metco (India) and Struers LaboPol-5 (Denmark) machines. The surface was polished using Struers MD Chem (Denmark) cloth polishing wheel with OP-S NonDry (SiC) suspension.

Before operation using an electron microscope, the polished surfaces were cleaned from impurities in a Sapphire ultrasound bath (35 kHz) in acetone in 15—30 min

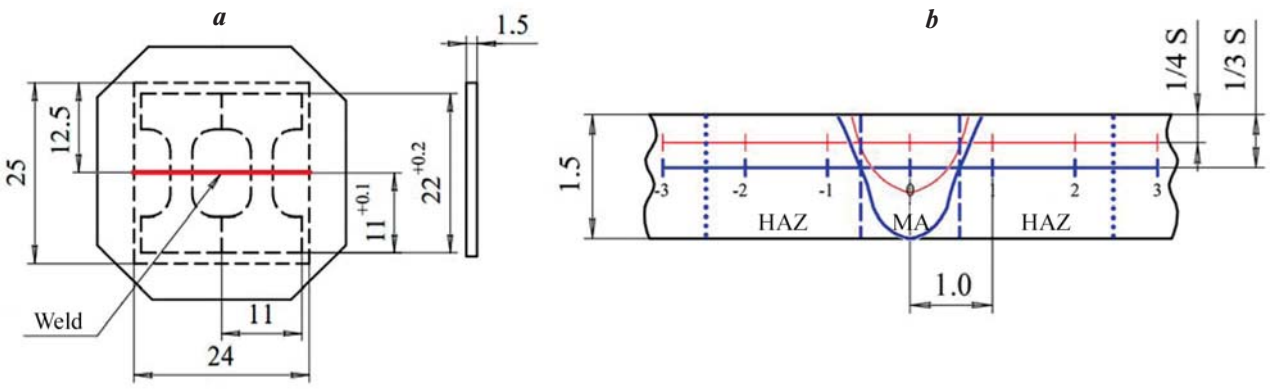

Fig. 3. Layout of sample preparation and microhardness measurement

a – cutting out of a sample from a forged workpiece for welding and subsequent uniaxial tensile testing;
b –measurement of microhardness in the cross section of the welded joint (0 – welded joint center)

Рис. 3. Схемы подготовки образцов и измерения микротвердости

a – резка образцов из поковки из сплава ВТИ-4 для сварки и последующих механических испытаний на одноосное растяжение;
b – измерение микротвердости в поперечном сечении сварного шва (0 – центр сварного шва)

with subsequent cleaning using a Plasma Cleaner Fischione machine (USA) in 30 min. The uniaxial tensile tests were performed using an Instron 5882 test machine (Great Britain) at ambient temperature at the loading rate of 10^{-3} s^{-1}.

Microhardness was determined on polished samples in transversal cross section of welded joints according to ISO 22826. The measurements were carried out with a step of 0.15 mm at a distance of 1/3 and 1/4 of the plate thickness depending on the depth of penetration (Fig. 3, *b*). The measurements were carried out using a Vickers 402MVD hardness meter (the Netherlands) with a load of 0.2 kg and an indentation time of 10 s ($HV_{0.2}$). Control and data acquisition were carried out using Hardtest Wolpert Group software (the Netherlands).

Microstructural studies were carried out using a Nova NanoSEM 450, FEI Q200 and Q600 3D microscopes (Czech Republic) equipped with backscattered electron detector (BSED) at accelerating voltage of 20—30 kV. Identification of geometrical patterns of structural areas of welded joints, data processing of phase and microtextural analyses were carried out using ImageJ and TSL OIM Analysis 9 software (USA). EBSD analysis was carried out in backscattered electron diffraction including recording of grain misorientation map. A sample for EBSD analysis was fixed at test table using carbon adhesive No. 502. A sample inclined at the angle of 70° to horizontal was scanned with the step of 1—3 μm by electron beam with the accelerating voltage of 20—30 kV.

Results and discussion

Description of initial material

The initial structure after multiaxial deformation of workpieces from the VTI-4 alloy is illustrated in Fig. 4. The microstructural studies in the transversal cross section of a sample processed by multiaxial forging revealed the homogeneous structure comprised of globular particles of α_2-phase with the diameter of 2—5 μm, laminar O-phase and fine grain β-matrix. The coarse primary grains of β-phase extended in the direction of final deformation are observed (see Fig. 4, *b*). They are fragmented into finer subgrains with the size of 15±2 μm (see Fig. 4, *a*). Along the boundaries of the latter, the globular particles of α_2-phase are located uniformly distributed over the volume. The plates of O-phase are present inside the subgrains of β-phase (see Fig. 4, *b*).

Visual Dimensional Inspection of Welded Joints

The external appearance of welded joint produced in various PLW modes is illustrated in Fig. 5. Using modes *1*, *2* and *4*, *5* (U = 280÷300 V, τ = 3÷6 ms), the WJ of a silver color were formed without significant convexities and shrinkage craters. Visually the welded points are of uniform round shape with fine flakiness (0.22±0.02 mm), the seam width: ~1.1 mm at pulse duration of 3 ms (see Fig. 5, *a—c*) and ~1.5 mm at 6 ms, respectively (see Fig. 5, *d—f*). However, upon a voltage increase to 320 V, on the WJ surface overlaps were detected as well as heterogene-

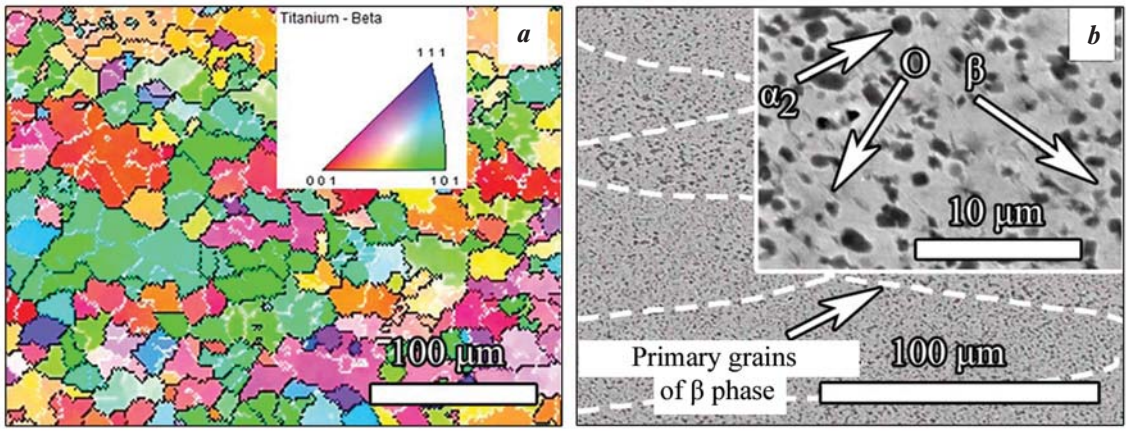

Fig. 4. Microstructure of forged workpiece from the VTI-4 alloy before pulsed laser beam welding

a – inverse pole figure map; ***b*** – BSE-SEM images of the microstructure after multiaxial deformation (the last deformation during multiaxial forging was vertical)

Рис. 4. Микроструктура кованой заготовки из сплава ВТИ-4 до проведения ИЛС

a – карта распределения ориентировок; ***b*** – снимки BSE-SEM микроструктуры после мультиосевой деформации (последняя деформация при мультиосевой ковке проходила вертикально)

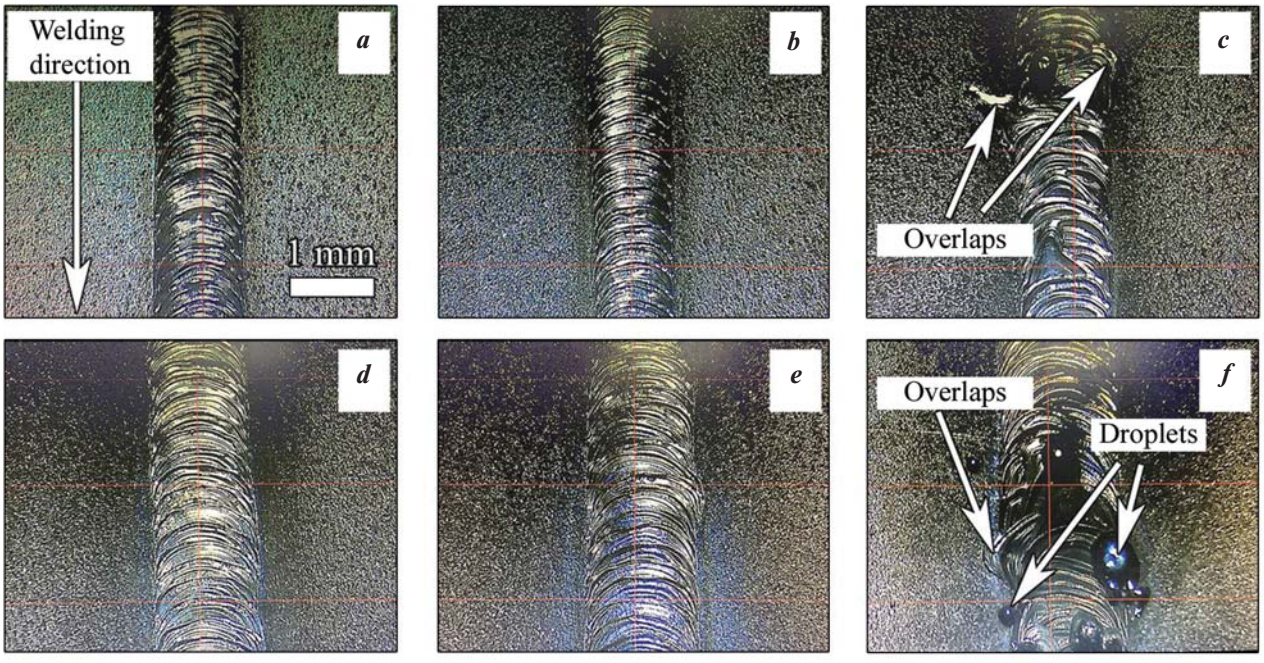

Fig. 5. Appearance of the welded joint from the VTI-4 alloy depending on the modes of laser welding, voltage and duration of the laser radiation pulse

a – mode *1*, ***b*** –*2*, ***c*** –*3*, ***d*** –*4*, ***e*** –*5*, ***f*** –*6*

Рис. 5. Внешний вид сварного соединения из сплава ВТИ-4 в зависимости от режимов ИЛС, напряжения и длительности импульса лазерного излучения

a – режим *1*, ***b*** – *2*, ***c*** –*3*, ***d*** – *4*, ***e*** – *5*, ***f*** – *6*

ous flakiness at τ = 3 ms (Fig. 5, *c*) and splashing at τ = 6 ms (Fig. 5, *f*).

High peak power and an increase in average pulse power lead to violation of thermal hydraulic processes of keyhole formation, promoting formation of coarse pores [22, 28], thus impairing the quality of welded joint. In addition, the energy density increases with pulse peak energy, and as is known, the higher the en-

ergy density, the more intensive is the collapse of bubbles, hence, the probability of formation of coarse pores increases [20].

Studying microstructure of welded joint

Transversal structure of welded joints produced in various PLW modes according to BSE-SEM and EBSD analyses is illustrated in Figs. 6 and 7. The transversal WJ was exposed from above to the impact of laser beam in pulsed mode with laser focusing on the surface of welded samples (focal distance is zero). The WJ shape is knife-like, characterized by the penetration depth and width (Fig. 8). The welded joint in the mode of knife fusion penetration is formed due to material evaporation and plasma formation on the surface. High temperatures on the surface and vapor pressure lead to expansion of the top part of WJ in comparison with its bottom part, thus forming a mushroom shape of the seam [29]. Fine internal pores with the diameter of 20—35 μm were detected. They are located mainly in the root and center of WJ (Fig. 6, *a*—*e*). First of all, occurrence of the pores is related with chemical activity of titanium alloys with respect to gases, which leads to formation of pores and

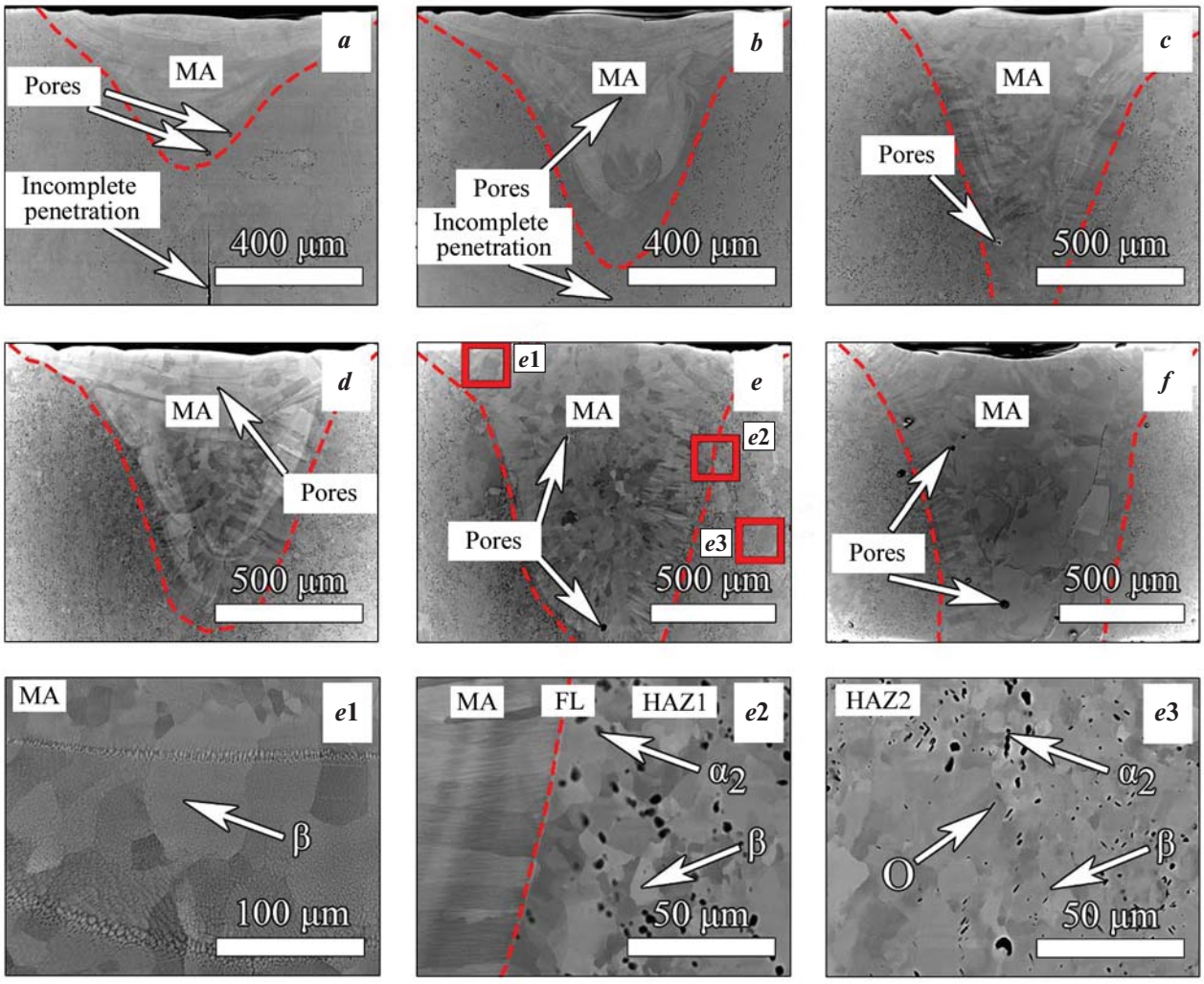

Fig. 6. Comparative analysis of microstructure of the welded joint from the VTI-4 alloy depending on the modes of pulsed laser beam welding

a – mode *1*, ***b*** –*2*, ***c*** –*3*, ***d*** –*4*, ***e*** –*5*, ***f*** –*6*
***e*1** – melting zone; ***e*2** – fusion line and first heat-affected zone; ***e*3** – second heat-affected zone

Рис. 6. Сравнительный анализ микроструктуры сварного соединения из сплава ВТИ-4 в зависимости от режимов ИЛС

a – режим *1*, ***b*** – *2*, ***c*** – *3*, ***d*** – *4*, ***e*** – *5*, ***f*** – *6*
***e*1** – зона плавления; ***e*2** – линия сплавления и первая зона термического влияния; ***e*3** – вторая зона термического влияния

cracks during welding [30]. Keyhole oscillations can cause more intensive formation of bubbles and their collapse will lead to formation of coarse pores and pores which do not have time to float remaining in the WJ central part [20].

When mode *6* is used (U = 320 V, τ = 6 ms), the number of transversal pores with a diameter of 40 ± ± 5 μm increases (Fig. 6, *f*). In addition, incomplete penetrations were detected in the seam root characteristic for modes with fusion depth of less than 1.5 mm (Fig. 6, *a*, *b*, *d*).

Figure *6* also illustrates that the welded joint has the melting area (MA) (Fig. 6, *e*1), the heat affected zone (HAZ), separated by the fusion line (FL), and the area of the base metal (BM) (Fig. 6, *e*2, e3).

It was established that the MA is comprised of β-phase, at the MA—FL interface the grains of β-phase have a more elongated shape, and with an increase in the average power of laser beam up to ~80 W their length increases from ~120 to ~190 μm (Fig. 7, *a—f*). With a further increase in the average power (mode *6*) the size of elongated grains of β-phase decreases to ~170 μm. This is attributed to better heat removal upon formation of opposite beam of the WJ root (Fig. 7, *f*). At the MA—FL interface α_2- and O-phases were completely dissolved upon heating and no back transformation took place upon cooling. At the boundary of the fusion line and HAZ1, there are no coarse globular grains of β-phase (Fig. 6, *e*2). Presumably, this is attributed to high temperature gradients stipulated by the PLW processes, when local impact of each pulse is accompanied by rapid cooling [31].

In turn, the area of thermal impact in terns of revealed structural constituents can be subdivided into HAZ1, comprised of β + α_2 phases (Fig. 6, *e*2), and HAZ2, structurally comprised of β + α_2 + O phases (Fig. 6, *e*3). In the HAZ1 area, the globular α_2-phase was partially retained, since for completion of $\alpha_2 \rightarrow \beta$ transformation higher temperatures are required [32]. Contrary to the base metal, in HAZ2 the O phase upon heating is partially transformed into β phase, whereas the α_2-phase is actually retained. Transition from HAZ1 to HAZ2 is gradual and accompanied by an increase in the fraction of the α_2-phase. During transition from HAZ2 to BM the fraction of the O-phase increases.

In center of the IPF EBSD maps cast, the structure of MA welded joint is observed. It is comprised mainly of elongated dendrites of β-phase, and in the FL region and in the central part of MA — of globular grains of β-phase

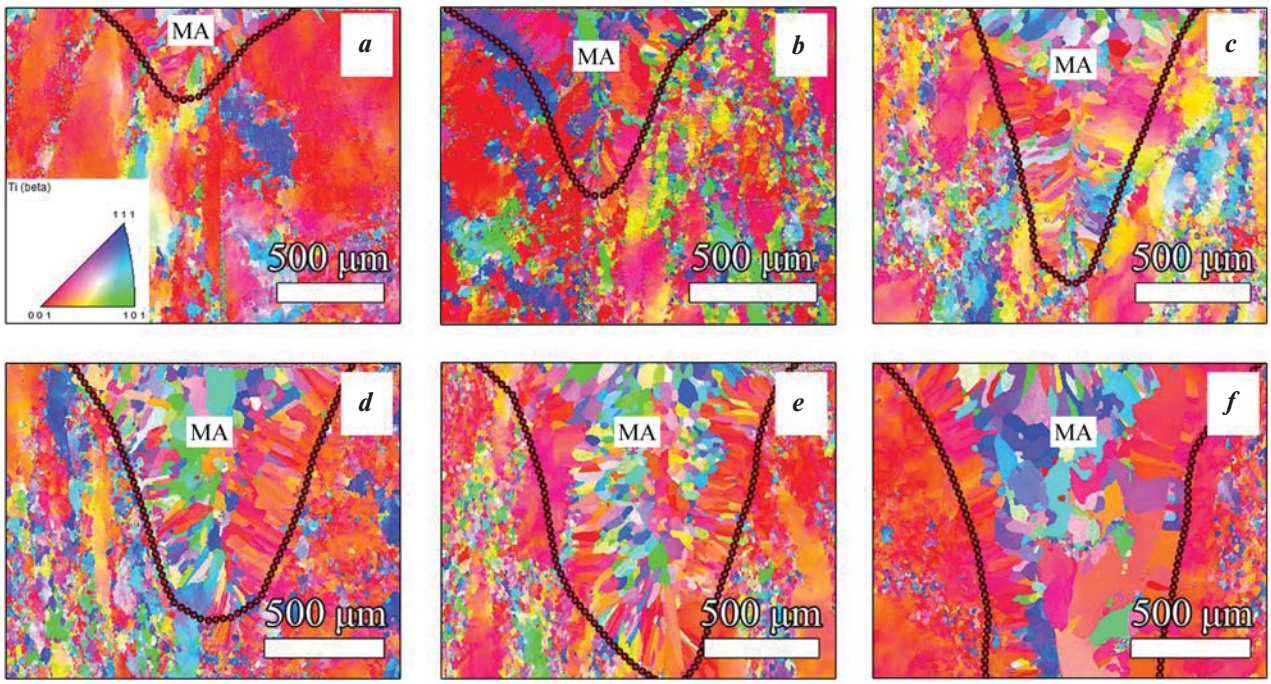

Fig. 7. EBSD analysis of welded joints from the VTI-4 alloy depending on PLW modes
a – mode *1*, ***b*** –*2*, ***c*** –*3*, ***d*** –*4*, ***e*** –*5*, ***f*** –*6*

Рис. 7. EBSD-анализ сварных соединений из сплава ВТИ-4 в зависимости от режимов ИЛС
a – режим *1*, ***b*** – *2*, ***c*** – *3*, ***d*** – *4*, ***e*** – *5*, ***f*** – *6*

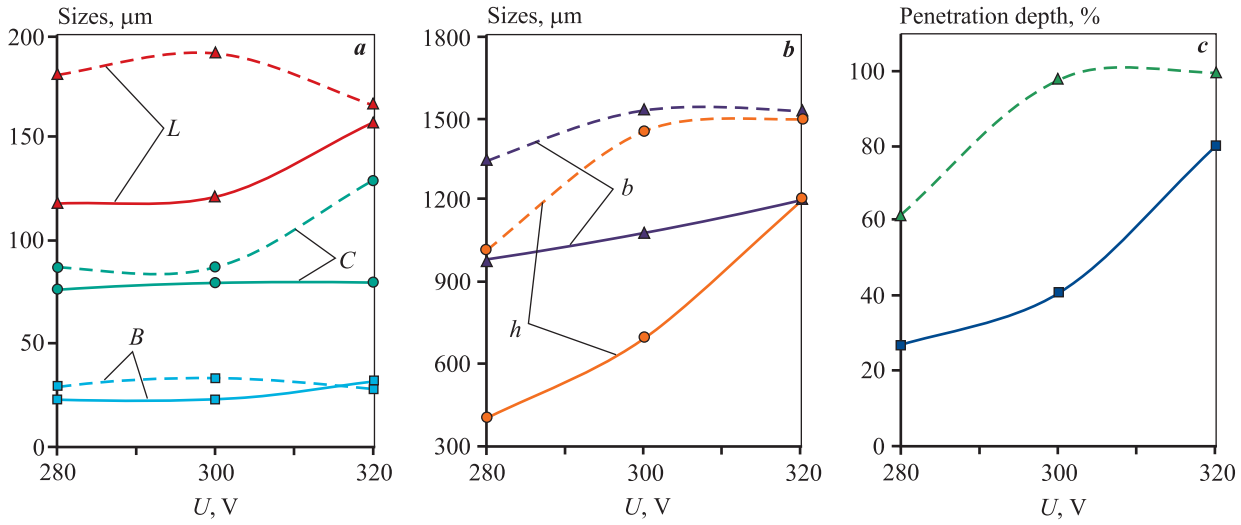

Fig. 8. Parameters of microstructure of welded joints from the VTI-4 alloy (***a***), their geometrical parameters (***b***) and penetration depth (***c***) depending on the PLW modes

τ = 3 ms (solid lines), τ = 6 ms (dashed lines)
a: *L* – length, *B* – width of dendrites at FL boundary, *C* – grain size
b: *h* – depth, *b* – width of the weld

Рис. 8. Параметры микроструктуры сварных швов из сплава ВТИ-4 (***a***), их геометрические параметры (***b***) и глубина проплавления (***c***) в зависимости от режимов ИЛС

τ = 3 мс (сплошные линии), τ = 6 мс (штриховые)
a: *L* – длина, *B* – ширина дендритов на границе ЛС, *C* – размер зерен
b: *h* – глубина, *b* – ширина сварного шва

(Fig. 7). The length of dendrites and the penetration depth increase from 119±20 to 192±15 μm with an increase in the laser power from 40 to 80 W. The width of elongated dendrites nearly does not change and retains in the range of 23—35 μm (Fig. 8, *a*). In welding mode *6* (U = 320 V, τ = 6 ms), the welding bath is deflected, the length of dendrites decreases to 167±15 μm, and their width in the central region of MA increases to 130±10 μm.

The peak power of laser beam influences not only on the penetration depth (Fig. 8, *a*), but also on the external shape of the seam. Usually in the case of repetitively pulsed lasers, the energy density reaches $E = 10^5 \div 10^7$ W/cm^2 at the pulse duration of $<10^{-3}$ s. At the peak power higher than 2.7 kW (Fig. 8, *b*) the energy density increases to $>10^7$, leading to violations in WJ formation, namely: splashing of liquid metal and overlaps (Fig. 5, *c*, *f*).

The width of welded joint at equal focal distance of laser depends on the duration of laser pulse impact: on average at τ = 3 ms it equals to 1.05±0.1 mm, at τ = 6 ms to 1.45±0.1 mm (Fig. 8, *b*). The penetration depth mostly depends on the laser energy density, at its peak power of 2.1 kW (Fig. 8, *c*) the penetration is 27 % of the thickness of welded plates; in welding mode *3* (U = 320 V, τ = 3 ms with the peak power of 3.2 kW) — 80 %. At a pulse duration of 6 ms and the voltage of 300 V and higher the complete penetration depth of plates from the VTI-4 alloy with the thickness of 1.5 mm is achieved (Fig. 8, *c*).

Studying mechanical properties of welded joints

The plots of microhardness and mechanical properties upon uniaxial tension of welded joints are illustrated in Figs. 9 and 10. The microhardness of transversal welded joints is about 340±20 $HV_{0.2}$, and that of base metal about 345±10 $HV_{0.2}$. In the HAZ region, the microhardness decreases to 330±5 $HV_{0.2}$. Generally, for Ti_2AlNb-based alloys, the dispersion strengthening of O-phase is the main mechanism of strengthening. Therefore, due to the absence of O-phase in the region of HAZ1 and MA, the microhardness is the lowest. While the extent of conversion of O-phase into B2-phase decreases from the welding area to HAZ2, the hardness profile demonstrates a trend towards an increase to the base metal [33, 34].

The variation of microhardness profiles in the HAZ1–2 region in comparison with BM and MA is related to changes in volumetric fraction and si-

zes of equiaxial phase α_2, which is mainly distributed along the boundaries of primary grains of β phase [35]. With an increase in the average laser power, the size of equiaxial α_2-phase (α_2 = 3.1±2.0 μm in BM) in HAZ nearly does not change from the average size of 2.8±2.0 μm (in welding mode *1*) to 2.5±2.0 μm (in welding mode *6*). The phase composition of α_2 in HAZ does not differ significantly from BM (~3 %

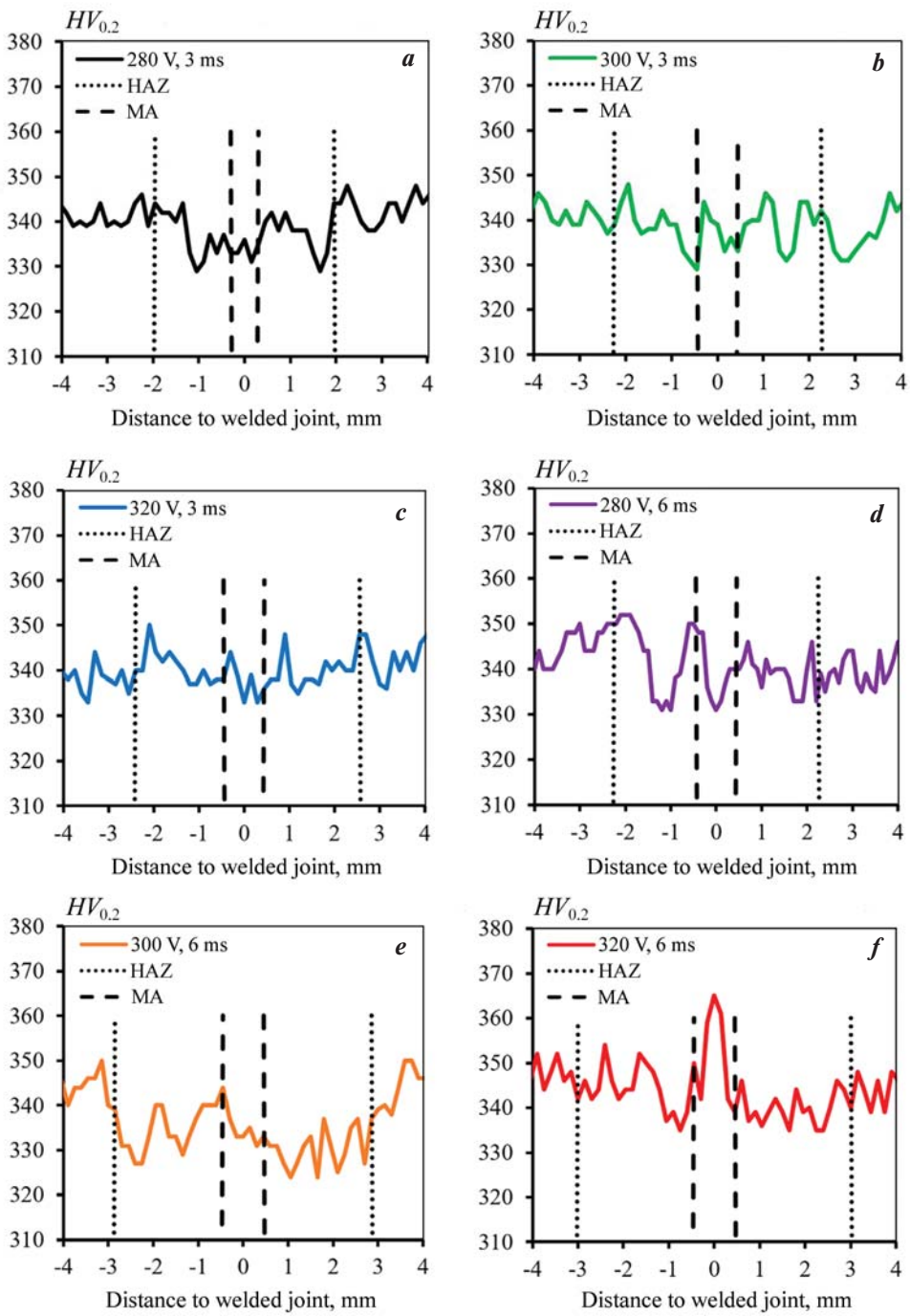

Fig. 9. Distribution of microhardness in the cross-section of welded joints from the VTI-4 alloy depending on PLW modes

a – mode *1*, ***b*** –*2*, ***c*** –*3*, ***d*** –*4*, ***e*** –*5*, ***f*** –*6*

Рис. 9. Распределение микротвердости в поперечном сечении сварных швов из сплава ВТИ-4 в зависимости от режимов ИЛС

a – режим *1*, ***b*** – *2*, ***c*** – *3*, ***d*** – *4*, ***e*** – *5*, ***f*** – *6*

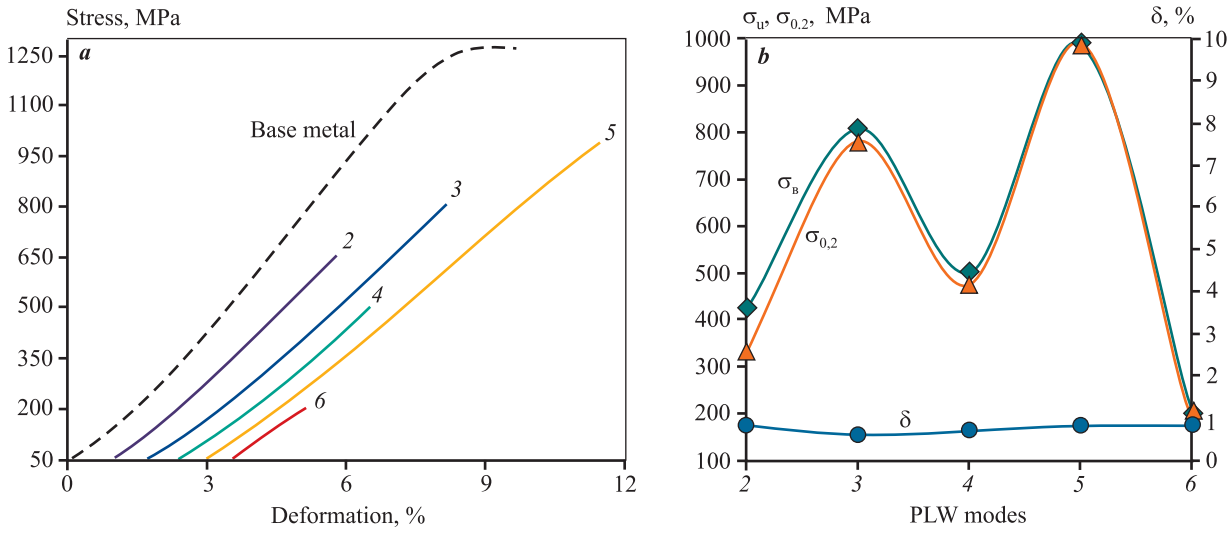

Fig. 10. Tensile diagram (***a***) and mechanical properties (***b***) of welded joints from the VTI-4 alloy depending on PLW modes (numbers near curves)

Рис. 10. Диаграмма растяжения (***a***) и механические свойства (***b***) сварных соединений из сплава ВТИ-4 в зависимости от режимов ИЛС (цифры у кривых)

α_2 phase), since in PLW modes *1—3* and *5* the fraction of α_2 in HAZ does not exceed 2.5 %, and in modes *4* and *6* — 3÷5 %.

Therefore, minor changes in the sizes, phase composition, and distribution of α_2-phase along the boundaries of primary grains of β-phase lead to variations in microhardness profiles transversal to WJ in various sites. Upon welding in mode *6* (U = 320 V, τ = 6 ms) in the MA region, a microhardness peak of 365 $HV_{0.2}$ can be observed. This is related to partial saturation with oxygen [36]. In this case gas was supplied along the laser impact on the surface of welded plates which does not eliminate completely the bath contact with ambient air from the side of seam root.

Mechanical properties of initial VTI-4 alloy are as follows: σ_u = 1250 MPa, $\sigma_{0.2}$ = 1200 MPa, δ = 2.07 %. The strength properties of welded joint are about 80 % of the strength of base metal are achieved at welding mode *5* (U = 300 V, τ = 6 ms). Further increase in the voltage up to 320 V leads to violation of PLW process and the occurrence of external defects, exerting a negative influence on the strength properties. With a decrease in the voltage to 280 V complete penetration (<70 % of the plate thickness) of welded joint is not achieved, and the strength is ~40 % of that of the base metal. The joint is not welded for full depth acts as the stress concentrator, thus impairing the strength properties.

The plasticity of welded joints in all cases decreases (Fig. 10, *b*), since the PLW as well as other method of fusion welding is accompanied by formation of coarse columnar B2 structure [13]. Plasticity can be increased by means of subsequent thermal treatment of welded joints [32].

Studying porosity in welded joint

Fractures after tensile tests are illustrated in Fig. 11. The sample thickness in Fig. 11, *a* was decreased due to localized heating on plate surface and its intensive deformation, as a consequence a portion of metal was removed as in Fig. 11, *e*, due to heterogeneity of welded joint, undercutting and metal splashing.

The fracture of welded joint in all cases is in the MA region closer to the FL boundary. On the fracture surface, a river relief is observed. On the fracture surface, the highest number of gaseous pores occurs (Fig. 11, *a—d*) and extended secondary cracks (Fig. 11, *a*1, *e*1) appear. Such microcracks are nucleated and propagated along the grain boundaries of β-phase due to the absence of deformation inside the grains. The fractures observed in this work are characteristic of the welded joints with the structure of β-phase, where during breaking the crack in the foundation of river line is split [13, 37].

The size and distribution of pores decrease with an increase in the laser power. At low heat input the coarse pores are concentrated on seam root. This is attributed to the violation of keyhole. With an increase in the energy the pore size decreases, the pores are distributed over

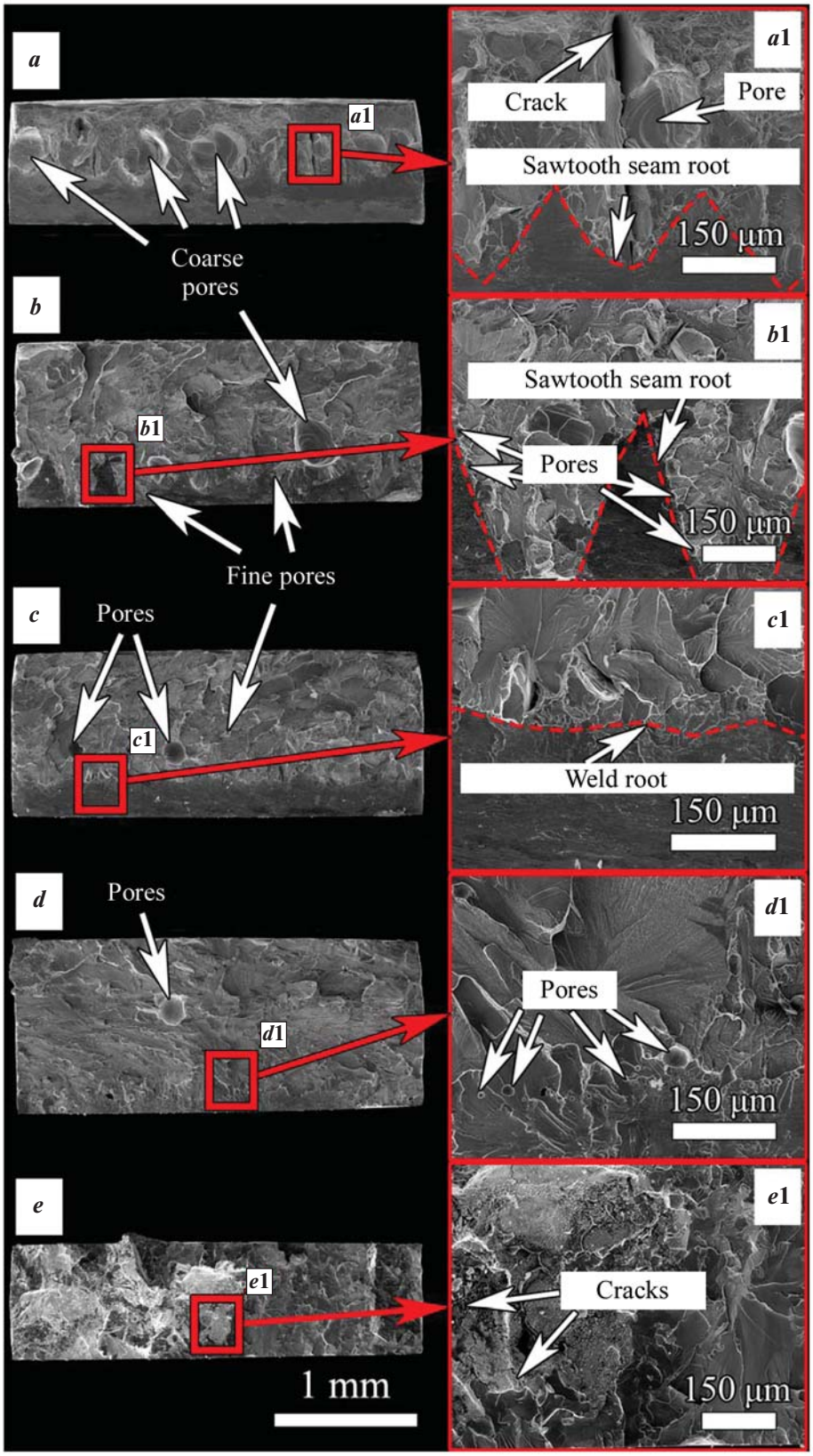

Fig. 11. Morphology of fracture surface of tensile specimens depending on PLW modes
a – mode *1*, ***b*** –*2*, ***c*** –*3*, ***d*** –*4*, ***e*** –*5*, ***f*** –*6* (impact of laser pulsed radiation from above)

Рис. 11. Морфологии поверхности излома образцов на растяжение в зависимости от режимов ИЛС
a – режим *1*, ***b*** – *2*, ***c*** – *3*, ***d*** – *4*, ***e*** – *5*, ***f*** – *6* (действие импульсного лазерного излучения сверху)

the entire volume providing more favorable conditions for floating of gas bubbles.

At the fracture of samples welded in mode *3* (U = = 320 V, τ = 3 ms), a sawtooth WJ root was detected, providing for complete penetration in some places (Fig. 11, *b*). Coarse pores are distributed non-uniformly over the fracture. In the WJ root and center, the high values of peak laser power with regard to its average exerts a negative impact on formation of keyhole. This leads to formation of coarse (Fig. 11, *b*) and fine (Fig. 11, *b*1) pores in the seam cross section [27].

Therefore, it can be seen (Fig. 11, *a*, *b*) that in the transversal cross section of a welded joint under the impact of short pulse and high voltages, the sawtooth seam root is more pronounced with the formation of coarser spherical pores with the sizes of 150—200 μm (modes *2* and *3*). With a twofold increase in the duration of the laser radiation pulse the sawtooth seam root is less pronounced (Fig. 11, *c*), and finer pores are formed: up to ~100 μm (mode *4*). Due to the stabilization of keyhole in mode *5* (U = 300 V, τ = 6 ms), maximum pore content is achieved using optimized welding parameters [38]. However, in mode *5*, fine spherical pores with the sizes of 10—30 μm are concentrated in the bottom part of the welded joint, which can be attributed to local incomplete penetration (Fig. 11, *d*1). The rare occurrence of single spherical pores with the size up to ~100 μm in the central part of transversal cross section of welded joint can be attributed to local incomplete penetration (Fig. 11, *d*).

Porosity decreases the effective surface area of welded joint cross section, makes it loose, decreases plasticity, and also acts as a stress concentrator [24]. This can be attributed to crack nucleation and its propagation to the WJ root in the welding mode *2* (U = = 300 V, τ = 3 ms) (Fig. 11, *a*1). Existence of coarse pores in welded joint cross section in modes *2* (~11.5 %) and 3 (~3.8 %) increases the volume of their total fraction in respect of fracture cross section (Fig. 11, *a*, *b*). With an increase in laser power and pulse duration, the fraction of pores in the transversal cross section decreases, equaling for mode *4* (U = 280 V, τ = 6 ms) to <2 % (average power: 60.8 W), and for the rest not higher than 1 %.

Conclusions

Due to the preliminary preparation of the structural state of material after multiaxial abc forging of a workpiece with heating up to 970 °C at the rate of <0.1 mm/s and deformation degree of 50 % in each case, as well as the use of optimum pulsed mode of laser welding, a faultless high quality welded joint was obtained from the Ti_2AlNb-based VTI-4 alloy with the strength properties at the level of ~80 % of the base metal.

In the case of the LAT-S-300 laser facility the optimum PLW conditions for sheet material from the VTI-4 alloy with the thickness of 1.5 mm, where the volumetric portion of pores does not exceed 1 % of the cross section of the welded joint, are as follows:

— pulse voltage: 300 V;
— pulse duration: 6 ms;
— step between pulses: 0.25 mm;
— flow rate of protecting gas: 2.5 bar;
— focal distance on the surface of workpieces is zero;
— welding speed: 0.3 m/min.

It was established that the melting area of the welded joint during PLW is comprised of β-phase, while α_2- and O-phases were completely dissolved upon heating. Due to the high temperature gradients stipulated by PLW processes, the heat affected zone is comprised of the of $\beta + \alpha_2$ and $\beta + \alpha_2 + O$ regions.

It was demonstrated that the reasons for the porosity of the welded joint upon PLW of the VTI-4 alloy are as follows:

— violations of thermal hydraulic processes;
— formation of sawtooth seam root with incomplete penetration;
— no protecting gas backing from the side of seam root;
— splashing of liquid metal;
— overlaps on seam surface;
— non-uniformity of pulse application.

All these factors lead to additional cracking, heterogeneity of the melting area and, as a consequence, to poorer mechanical properties.

References

1. Banerjee D., Gogia A.K., Nandi T.K., Joshi V.A. A new ordered orthorhombic phase in a Ti_3AlNb alloy. *Acta Metallurgica*. 1988;36(4):871—882. https://doi.org/10.1016/0001-6160(88)90141-1
2. Banerjee D. The intermetallic Ti_2AlNb. *Progress in Materials Science*. 1997;42(1-4):135—158. https://doi.org/10.1016/S0079-6425(97)00012-1
3. Wang L., Sun D., Li H., Gu X., Shen C. Microstructures and mechanical properties of a laser-welded joint of Ti_3Al—Nb alloy using pure Nb filler metal. *Metals (Basel)*. 2018;8(10):785. https://doi.org/10.3390/met8100785
4. Shagiev M.R., Galeyev R.M., Valiakhmetov O.R. Ti_2AlNb-Based intermetallic alloys and composites. *Materials physics and mechanics*. 2017;33(1):12—18. https://doi.org/10.18720/MPM.3312017_2

5. Pollock T.M., Tin S. Nickel-based superalloys for advanced turbine engines: Chemistry, microstructure, and properties. *Journal of Propulsion and Power*. 2006;22(2):361—374. https://doi.org/10.2514/1.18239
6. Liu X., Wu S., Ji Y., Shao L., Zhao H., Wan X. Ultrasonic frequency pulse tungsten inert gas welding of Ti_2AlNb-based alloy. *Xiyou Jinshu/Chinese Journal of Rare Metals*. 2014;38(4):541—547. https://doi.org/10.13373/j.cnki.cjrm.2014.04.001
7. Lu B., Yin J., Wang Y., Yang R. Gas tungsten arc welding of Ti_2AlNb based alloy sheet. In: *Proc. 12th World Conf. Titan (Ti 2011)*. (China, Beijing, 19—24 June 2011). 2012. Vol. 1. P. 816—818.
8. Shao L., Cui E. Joining of Ti—22Al—25Nb Alloy using different welding methods. *Materials China*. 2019;38(3):286—290. https://doi.org/10.7502/j.issn.1674-3962.2019.03.11
9. Mohandas T., Banerjee D., Mahajan Y.R., Kutumba Rao V.V. Studies on fusion zone fracture behaviour of electron beam welds of an α + β-titanium alloy. *Journal of Materials Science*. 1996;31(14):3769—3775. https://doi.org/10.1007/BF00352792
10. Li D., Hu S., Shen J., Zhang H., Bu X. Microstructure and mechanical properties of laser-welded joints of Ti—22Al—25Nb/TA15 dissimilar titanium alloys. *Journal of Materials Engineering and Performance*. 2016;25(5):1880—1888. https://doi.org/10.1007/s11665-016-2025-4
11. Li Y.-J., Wu Ai-P., Li Q., Zhao Y., Zhu R.-C., Wang G.-Q. Effects of welding parameters on weld shape and residual stresses in electron beam welded Ti_2AlNb alloy joints. *Transactions of Nonferrous Metals Society of China*. 2019;29(1):67—76. https://doi.org/10.1016/S1003-6326(18)64916-7
12. Skupov A.A., Sviridov A.V., Khodakova E.A., Afanasev-Khodykin A.N. Creation of joints from intermetallic titanium alloys (review). *Trudy VIAM*. 2021;7:31—38. (In Russ.).
Скупов А.А., Свиридов А.В., Ходакова Е.А., Афанасьев-Ходыкин А.Н. Создание неразъемных соединений из интерметаллидных титановых сплавов (обзор). *Труды ВИАМ*. 2021;7:31—38. https://doi.org/10.18577/2307-6046-2021-0-7-31-38
13. Zhang K., Lei Z., Chen Y., Yang K., Bao Y. Heat treatment of laser-additive welded Ti_2AlNb joints: Microstructure and tensile properties. *Materials Science and Engineering: A*. 2019;744:436—444. https://doi.org/10.1016/j.msea.2018.12.058
14. Auwal S.T., Ramesh S., Yusof F., Manladan S.M. A review on laser beam welding of titanium alloys. International *Journal of Advanced Manufacturing Technology*. 2018;97(1-4):1071—1098. https://doi.org/10.1007/s00170-018-2030-x
15. Chludzinski M., dos Santos R.E., Churiaque C., Ortega-Iguña M., Sánchez-Amaya J.M. Pulsed laser welding applied to metallic Materials — A Material Approach. *Metals*. 2021;21(4):640. https://doi.org/10.3390/met11040640
16. Zhang P., Jia Z., Yu Z., Shi H., Li S., Wu D., Yan H., Ye X., Chen J., Wang F., Tian Y. A review on the effect of laser pulse shaping on the microstructure and hot cracking behavior in the welding of alloys. *Optics & Laser Technology*. 2021;140:107094. https://doi.org/10.1016/j.optlastec.2021.107094
17. Gaikwad A., Deore H., Kotwal V., Pawar A., Valli A. Review on laser welding of titanium alloy. In: *Proc. International Conference on Ideas, Impact and Innovation in Mechanical Engineering (ICIIIME 2017)* (India, Rajasthan, 1—2 June 2017). 2017. Vol. 5(6). P. 789—795.
18. Li Y.-J., Wu A.-P., Li Q., Zhao Y., Zhu R.-C., Wang G.-Q. Mechanism of reheat cracking in electron beam welded Ti_2AlNb alloys. *Transactions of Nonferrous Metals Society of China*. 2019;29(9):1873—1881. https://doi.org/10.1016/S1003-6326(19)65095-8
19. Panov D.O., Naumov S.V., Sokolovsky V.S., Volokitina E.I., Kashaev N., Ventzke V., DInse R., Riekehr S., Povolyaeva E.A., Alekseev E.B., Nochovnaya N.A., Zherebtsov S.V., Salishchev G.A. Cracking of Ti_2AlNb-based alloy after laser beam welding. *IOP Conference Series: Materials Science and Engineering*. 2021;1014:012035. https://doi.org/10.1088/1757-899X/1014/1/012035
20. Xu J., Rong Y., Huang Y., Wang P., Wang C. Keyhole-induced porosity formation during laser welding. *Journal of Materials Processing Technology*. 2018;252:720—727. https://doi.org/10.1016/j.jmatprotec.2017.10.038
21. Zhou J., Tsai H.L. Porosity formation and prevention in pulsed laser welding. *ASME Journal of Heat and Mass Transfer*. 2007;129(8):1014—1024. https://doi.org/10.1115/1.2724846
22. Bruyere V., Touvrey C., Namy P. A phase field approach to model laser power control in spot laser welding. In: *Proc. 2014 COMSOL Conf. 2014*. P. 1—4. URL: https://www.comsol.com/paper/a-phase-field-approach-to-model-laser-power-control-in-spot-laser-welding-18505 (accessed: 01.09.2022).
23. Li H. Analysis of porosity in welding of titanium alloy. In: *Proc. 2020 3rd International Conference on Electron Device and Mechanical Engineering (ICEDME)* (China, Suzhou, 1—3 May 2020). 2020. P. 486—489. https://doi.org/10.1109/ICEDME50972.2020.00116
24. Li H. The causes and control of porosity in titanium alloy welding. In: *Proc. 2020 3rd International Conference on Electron Device and Mechanical Engineering (ICEDME)* (China, Suzhou, 1—3 May 2020). 2020. P. 490—493. https://doi.org/10.1109/ICEDME50972.2020.00117

25. Huang J.L., Warnken N., Gebelin J.-C., Strangwood M., Reed R.C. On the mechanism of porosity formation during welding of titanium alloys. *Acta Materialia*. 2012;60(6-7):3215—3225. https://doi.org/10.1016/j.actamat.2012.02.035
26. Chen W., Li J.W., Xu L., Lu B. Development of Ti_2AlNb alloys: Opportunities and challenges. *Advanced Materials and Processes*. 2014;172(5):23—27.
27. Zhan X., Yan T., Gao Q., Zhu Z., Bu H., Wang Z. The porosity formation mechanism in the laser welded joint of TA15 titanium alloy. *Materials Research Express*. 2019;6(7):076558. https://doi.org/10.1088/2053-1591/ab1612
28. Torkamany M.J., Malek Ghaini F., Papan E., Dadras S. Process optimization in titanium welding with pulsed Nd:YAG laser. *Science of Advanced Materials*. 2012;4(3-4): 489—496. https://doi.org/10.1166/sam.2012.1307
29. Baranov D.A., Parkin A.A., Zhatkin S.S. Features of formation of the welded seam of heat-resistant KhN45VMTYuBR alloy depending on the modes of laser welding. *Izvestiya Samarskogo nauchnogo tsentra RAN*. 2018;2:170—176. (In Russ.).
Баранов Д.А., Паркин А.А., Жаткин С.С. Особенности формирования сварного шва жаропрочного сплава ХН45ВМТЮБР в зависимости от режимов лазерной сварки. *Известия Самарского научного центра РАН*. 2018;2:170—176.
30. Grigoryants A.G., Shiganov I.N., Misyurov A.I. Technological processes of laser processing. Moscow: MGTU imeni. N.E. Baumana. 2008. 664 p. (In Russ.).
Григорьянц А.Г., Шиганов И.Н., Мисюров А.И. Технологические процессы лазерной обработки. Москва: МГТУ им. Н.Э. Баумана, 2008. 664 с.
31. Baeslack W.A., Cieslak M.J., Headley T.J. Structure, properties and fracture of pulsed Nd:YAG laser welded Ti—14.8wt%Al—21.3wt%Nb titanium aluminide. *Scripta Metallurgica*. 1988;22(7):1155—1160. https://doi.org/10.1016/S0036-9748(88)80122-4
32. Panov D., Naumov S., Stepanov N., Sokolovsky V., Volokitina E., Kashaev N., Ventzke V., Dinse R., Riekehr S., Povolyaeva E., Nochovnaya N., Alekseev E., Zherebtsov S., Salishchev G. Effect of pre-heating and post-weld heat treatment on structure and mechanical properties of laser beam-welded Ti_2AlNb-based joints. *Intermetallics*. 2022;143:107466. https://doi.org/10.1016/j.intermet.2022.107466
33. Chen X., Xie F. Q., Ma T. J., Li W. Y., Wu X. Q. Effects of post-weld heat treatment on microstructure and mechanical properties of linear friction welded Ti_2AlNb alloy. *Materials & Design*. 2016;94:45—53. https://doi.org/10.1016/j.matdes.2016.01.017
34. Xiong L., Mi G., Wang C. Microstructure and mechanical properties of laser-welded joints of Ti—22Al-25Nb/Ti—6Al—4V dissimilar titanium alloys. *Journal of Laser Applications*. 2018;30(3):032412. https://doi.org/10.2351/1.5040610
35. Chen W., Chen Z.Y., Wu C.C., Li J.W., Tang Z.Y., Wang Q.J. The effect of annealing on microstructure and tensile properties of Ti—22Al—25Nb electron beam weld joint. *Intermetallics*. 2016;75:8—14. https://doi.org/10.1016/j.intermet.2016.02.006
36. Mehdi B., Badji R., Ji V., Allili B., Bradai D., Deschaux-Beaume F., Soulié F. Microstructure and residual stresses in Ti—6Al—4V alloy pulsed and unpulsed TIG welds. *Journal of Materials Processing Technology*. 2016;231:441—448. https://doi.org/10.1016/j.jmatprotec.2016.01.018
37. Wu J., Xu L., Lu Z., Cui Y., Yang R. Preparation of powder metallurgy Ti—22Al—24Nb—0.5Mo alloys and electron beam welding. *Jinshu Xuebao/ Acta Metallurgica Sinica*. 2016;52:1070—1078. https://doi.org/10.11900/0412.1961.2016.00019
38. Huang J., Turner R., Gebelin J.C., Warnken N., Strangwood M., Reed R.C. The effect of hydrogen on porosity formation during electron beam welding of titanium alloys. In: *ASM Proc International Conference on Trends in Welding Rearch* (USA, Chicago, 4—8 June 2012). 2013. P. 868—875.

Information about the authors

Stanislav V. Naumov – Cand. Sci. (Eng.), Assistant Professor of the Department of Materials Science and Nanotechnology (MSN); Senior Research Scientist of the Laboratory of Bulk Nanostructured Materials (BNM), Belgorod State University (BSU).
https://orcid.org/0000-0002-4084-8861
E-mail: NaumovStanislav@yandex.ru

Dmitrii O. Panov – Cand. Sci. (Eng.), Assistant Professor of the Department of MSN; Senior Research Scientist of the Laboratory of BNM, BSU.
https://orcid.org/0000-0002-8971-1268
E-mail: dimmak-panov@mail.ru

Ruslan S. Chernichenko – Engineer of the Laboratory of BNM, BSU.
https://orcid.org/0000-0002-8619-0700
E-mail: chernichenko@bsu.edu.ru

Vitaly S. Sokolovsky – Cand. Sci. (Eng.), Research Scientist of the Laboratory of BNM, BSU.
https://orcid.org/0000-0001-5607-2765
E-mail: sokolovskiy@bsu.edu.ru

Elena I. Volokitina – Engineer of the Laboratory of BNM, BSU.
https://orcid.org/0000-0001-9554-2651
E-mail: 1108668@bsu.edu.ru

Nikita D. Stepanov – Cand. Sci. (Eng.), Assistant Professor of the Department of MSN; Senior Research Scientist of the Laboratory of BNM, BSU.
https://orcid.org/0000-0003-2476-3953
E-mail: stepanov@bsu.edu.ru

Sergey V. Zherebtsov – Dr. Sci. (Eng.), Professor of the Department of MSN, Chief Research Scientist of the Laboratory of BNM, BSU.
https://orcid.org/0000-0002-1663-429X
E-mail: zherebtsov@bsu.edu.ru

Evgeny B. Alekseev – Cand. Sci. (Eng.), Head of Sector, All-Russia Institute of Aviation Materials «VIAM».
Scopus-ID 56581528500
E-mail: hiten_@mail.ru

Nadezhda A. Nochovnaya – Dr. Sci. (Eng.), Head of Laboratory, All-Russia Institute of Aviation Materials «VIAM».
E-mail: nochovnaya_viam@mail.ru

Gennady A. Salishchev – Dr. Sci. (Eng.), Professor of the Department of MSN, Head of the Laboratory of BNM, BSU.
https://orcid.org/0000-0002-0815-3525
E-mail: salishchev_g@bsu.edu.ru

Информация об авторах

Станислав Валентинович Наумов – к.т.н., доцент кафедры материаловедения и нанотехнологий (МиН), ст. науч. сотрудник лаборатории объемных наноструктурных материалов (ОНМ), Белгородский государственный национальный исследовательский университет (НИУ «БелГУ»).
https://orcid.org/0000-0002-4084-8861
E-mail: NaumovStanislav@yandex.ru

Дмитрий Олегович Панов – к.т.н., доцент кафедры МиН, ст. науч. сотрудник лаборатории ОНМ, НИУ «БелГУ».
https://orcid.org/0000-0002-8971-1268
E-mail: dimmak-panov@mail.ru

Руслан Сергеевич Черниченко – инженер лаборатории ОНМ, НИУ «БелГУ».
https://orcid.org/0000-0002-8619-0700
E-mail: chernichenko@bsu.edu.ru

Виталий Сергеевич Соколовский – к.т.н., науч. сотрудник лаборатории ОНМ, НИУ «БелГУ».
https://orcid.org/0000-0001-5607-2765
E-mail: sokolovskiy@bsu.edu.ru

Елена Ивановна Волокитина – инженер лаборатории ОНМ, НИУ «БелГУ».
https://orcid.org/0000-0001-9554-2651
E-mail: 1108668@bsu.edu.ru

Никита Дмитриевич Степанов – к.т.н., доцент кафедры МиН, ст. науч. сотрудник лаборатории ОНМ, НИУ «БелГУ».
https://orcid.org/0000-0003-2476-3953
E-mail: stepanov@bsu.edu.ru

Сергей Валерьевич Жеребцов – д.т.н., профессор кафедры МиН, гл. науч. сотрудник лаборатории ОНМ, НИУ «БелГУ».
https://orcid.org/0000-0002-1663-429X
E-mail: zherebtsov@bsu.edu.ru

Евгений Борисович Алексеев – к.т.н., начальник сектора, Всероссийский научно-исследовательский институт авиационных материалов (ВИАМ).
Scopus-ID: 56581528500
E-mail: hiten_@mail.ru

Надежда Алексеевна Ночовная – д.т.н., начальник лаборатории, ВИАМ.
E-mail: nochovnaya_viam@mail.ru

Геннадий Алексеевич Салищев – д.т.н., профессор кафедры МиН, зав. лабораторией ОНМ, НИУ «БелГУ».
https://orcid.org/0000-0002-0815-3525
E-mail: salishchev_g@bsu.edu.ru

Contribution of the authors

S.V. Naumov – planned and conducted experiments, wrote an article.

D.O. Panov – carried out forging, participated in the discussion of the results, corrected the article.

R.S. Chernichenko – prepared initial samples, prepared samples for research, conducted mechanical tests.

V.S. Sokolovsky – conducted EBSD analysis, conducted experiments, corrected the article.

E.I. Volokitina – prepared samples for structural studies.

N.D. Stepanov – participated in the discussion of the results.

S.V. Zherebtsov – participated in the discussion of the results.

E.B. Alekseev – produced the initial alloy for experiments.

N.A. Nochovnaya – determined the purpose of the work, produced the initial alloy for experiments.

G.A. Salishchev – determined the purpose of the work, participated in the discussion of the results, corrected the article.

Вклад авторов

С.В. Наумов – планирование и проведение экспериментов, подготовка текста.

Д.О. Панов – проведение ковки, участие в обсуждении результатов, правка статьи.

Р.С. Черниченко – подготовка исходных образцов и образцов для исследований, проведение механических испытаний.

В.С. Соколовский – проведение EBSD анализа, проведение экспериментов, правка статьи.

Е.И. Волокитина – подготовка образцов для структурных исследований.

Н.Д. Степанов – участие в обсуждении результатов.

С.В. Жеребцов – участие в обсуждении результатов.

Е.Б. Алексеев – приготовление исходного сплава для экспериментов.

Н.А. Ночовная – определение цели работы, изготовление исходного сплава для экспериментов.

Г.А. Салищев – научное руководство, участие в обсуждении результатов, правка статьи.

The article was submitted 03.09.2022, revised 08.03.2023, accepted for publication 10.03.2023

Статья поступила в редакцию 03.09.2022, доработана 08.03.2023, подписана в печать 10.03.2023